J. Fluid Mech. (2007), *vol.* 590, *pp.* 381–409.
doi:10.1017/S0022112007008117 Printed in the United Kingdom

Iso-surface mass flow density and its implications for turbulent mixing and combustion

SEUNG HYUN KIM[1] AND ROBERT W. BILGER[2]

[1]Center for Turbulence Research, Stanford University, Stanford CA 94305-3035, USA

[2]School of Aerospace, Mechanical and Mechatronic Engineering, The University of Sydney, Sydney, NSW 2003, Australia

(Received 23 April 2007 and in revised form 21 June 2007)

A new result is derived for the mass flow rate per unit volume through a scalar iso-surface – called here the 'iso-surface mass flow density'. The relationship of the surface mass flow density to the local entrainment rate per unit volume in scalar mixing and to the local reaction rate in turbulent premixed combustion is considered. In inhomogeneous flows, integration of the surface mass flow density across the layer in the direction of the mean scalar inhomogeneity yields the mean entrainment velocity in scalar mixing and the turbulent burning velocity in premixed combustion. For non-premixed turbulent reacting flow, this new result is shown to be consistent with the classical result of Bilger (*Combust. Sci. Technol.* vol. 13, 1976, p. 155) for fast one-step irreversible chemical reactions. Direct numerical simulation data for conserved scalar mixing, isothermal reaction front propagation and turbulent premixed flames are analysed. It is found that the entrainment velocity in the conserved scalar mixing case is sensitive to a threshold value. This suggests that the entrainment velocity is not a well-defined concept in temporally developing mixing layers and that scaling laws for the viscous superlayer warrant further investigation. In the isothermal reaction fronts problem, the characteristics of iso-surface propagation in a low Damköhler number regime are investigated. In premixed flames, the effects of non-stationarity on the turbulent burning velocity are addressed. The difference from the existing methods for determining turbulent burning velocity, and the implications of the present results for flames with multi-dimensional complex geometry are discussed. It is also shown that the surface mass flow density is related to the turbulent scalar flux in statistically stationary one-dimensional premixed flames. Variations of the local propagation characteristics due to departure from an unstretched laminar flame structure are shown to decrease the tendency to counter-gradient transport in turbulent premixed flames.

1. Introduction

The study of the behaviour of iso-scalar surfaces is crucial in understanding turbulent mixing and combustion. Iso-surfaces in turbulent flows are complicated owing to stretching and folding by random velocity fluctuations with a broadband spectrum of time and length scales (Candel & Poinsot 1990; Trouve & Poinsot 1994; Vervisch *et al.* 1995). Increased surface area and scalar gradients due to the turbulent motions result in the enhanced mixing of the scalar. Overall reaction rates in turbulent non-premixed combustion increase with the turbulent mixing rate, when there is little local extinction. The propagation of iso-surfaces is of critical importance in turbulent

premixed combustion, where the flame fronts can be defined as iso-surfaces of a reactive scalar.

In this work, existing results for the velocity of the fluid relative to a scalar isosurface (Gibson 1968; Pope 1988) and of the fine-grained density of the surface area of the iso-surface (Pope 1990; Vervisch *et al.* 1995) are combined to give a new result for the mass flow rate per unit volume through the iso-surface, called here the '*surface mass flow density*'. The relationship of the surface mass flow density to the local entrainment rate per unit volume in scalar mixing and to the local reaction rate in turbulent premixed combustion is considered. In inhomogeneous flows, integration of the surface mass flow density across the layer in the direction of the mean scalar inhomogeneity yields the mean entrainment velocity in scalar mixing and the turbulent burning velocity in premixed combustion.

In non-premixed turbulent combustion with a fast one-step irreversible reaction, the reaction rate per unit volume is given by Bilger (1976). The iso-surface mass flow density derived here is shown to be consistent with this result.

The concept of entrainment in turbulent mixing is well established (Pope 2000). Often the entrainment is expressed in terms of the entrainment of a scalar quantity. Questions remain, however, as to the sensitivity of the result to the threshold value chosen for the scalar. This is similar to the question of the effect of the threshold on the evaluation of scalar intermittency (Bilger, Antonia & Srinivasan 1976). The results derived here for the surface mass flow density and the entrainment velocity allow a more satisfactory framework for addressing these questions. Direct numerical simulations of a temporally developing scalar mixing layer have been carried out to explore this issue.

The concept of turbulent burning velocity in premixed combustion is well established (Peters 2000), but appears to be only well-defined in the ideal situation of a flame brush that is statistically one-dimensional and stationary in the mean (Cheng & Shepherd 1991; Bilger *et al.* 2005). Experimental methods of determining turbulent burning velocity (Peters 2000) include spherical propagation in a fan-stirred combustion vessel, flames stabilized on a Bunsen burner, turbulent counterflow premixed flames and flames stabilized in a weakly swirling co-flow. Results depend on the choice of method to define the location of the flame front and can arise from the time-developing nature of the flame brush propagation and/or the divergent nature of the flow. The results derived here for the surface mass flow density and the turbulent burning velocity allow a more satisfactory framework for addressing such questions. Direct numerical simulations of developing planar isothermal reaction fronts and turbulent premixed flames have been carried out to explore the issues associated with non-stationarity.

Swaminathan, Bilger & Ruetch (1997) have shown that the turbulent scalar flux in turbulent premixed flames is related to the structure of the instantaneous flame front. The results derived here for the surface mass flow density are used to further elucidate the transition from countergradient to gradient behaviour of the turbulent scalar flux.

The paper is organized as follows. In § 2, the mathematical formulation of the surface mass density is presented together with results for the total mass flux across inhomogeneous layers, entrainment velocity and turbulent burning velocity. It is verified that this new result is consistent with the classical result for fast one-step irreversible chemical reactions in non-premixed turbulent reacting flow. In § 3, the methods employed in the direct numerical simulations are outlined together with the parameters used for the cases studied. Results arising from the direct numerical

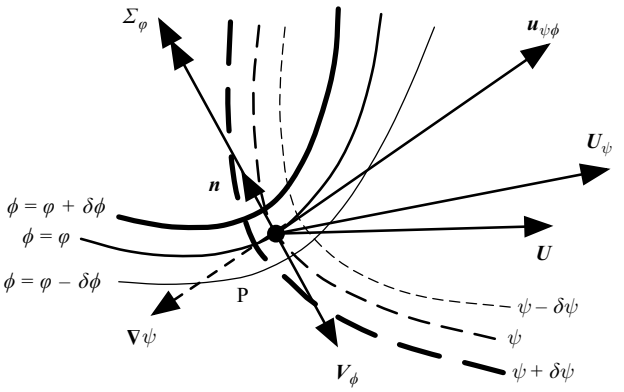

FIGURE 1. Local scalar fields ϕ and ψ at time t near the point P in a particular member of the complete ensemble of turbulent flows and the associated vectors of interest at point P. The fluid velocity at P is $\boldsymbol{U}$; $\boldsymbol{U}_\psi$ is the velocity of species ψ; $\boldsymbol{V}_\phi$ is the velocity of the iso-surface with a fixed value of ϕ, here coincidentally equal to φ; $\boldsymbol{n}$ is the unit normal to that iso-surface and $\boldsymbol{\Sigma}_\varphi$ its 'fine-grained' surface density, the double arrowhead denoting its delta-function-like character. The velocity of scalar ψ relative to the iso-surface is $\boldsymbol{u}_{\psi\phi}$.

simulations are presented and discussed in § 4. Further discussion on turbulent burning velocity and implications for multi-dimensional flames is presented in § 5, and the paper ends with a summary of the main conclusions.

2. Theory

2.1. *Iso-surface mass flow density*

Our task here is to derive general results for the flow of a scalar ψ through the iso-surface of another scalar ϕ upon which ϕ has the value φ. Results for the special cases when ψ and ϕ are the same and when $\psi = 1$ are also to be obtained.

Figure 1 shows schematically the local scalar fields near a point P at time t in a particular member of the total ensemble of this turbulent mixing flow. Also shown are the vectors of interest in this analysis. The scalar ϕ is denoted by solid curves with the line thickness denoting the magnitude of ϕ, while the scalar ψ is denoted by dashed curves with magnitude also denoted by line thickness. The depiction coincides with the condition that $\phi = \varphi$ at P.

The rate of displacement $\boldsymbol{V}_\phi$ of a constant property surface with scalar $\phi = \varphi$ is given by

$$\boldsymbol{V}_\phi = \frac{-\boldsymbol{n}(\partial\phi/\partial t)}{|\nabla\phi|} + \boldsymbol{V}_\phi^t, \tag{2.1}$$

where $\boldsymbol{n} = \nabla\phi/|\nabla\phi|$ is the unit vector normal to the constant property surface, positive in the direction of increasing ϕ (de Goey & Boonkkamp 1999), and $\boldsymbol{V}_\phi^t$ is the velocity component tangential to the constant property surface. For the other scalar, ψ, its velocity in the laboratory frame is, assuming Fickian diffusion,

$$\boldsymbol{U}_\psi = \boldsymbol{U} - \frac{D_\psi}{\psi}\nabla\psi, \tag{2.2}$$

so that the velocity of the scalar ψ relative to the iso-surface is given by (2.2)–(2.1)

$$\boldsymbol{u}_{\psi\phi} = \boldsymbol{U}_\psi - \boldsymbol{V}_\phi = \boldsymbol{U} - \frac{D_\psi}{\psi}\nabla\psi - \frac{-\boldsymbol{n}(\partial\phi/\partial t)}{|\nabla\phi|} - \boldsymbol{V}_\phi^t = \frac{\boldsymbol{n}(D\phi/Dt)}{|\nabla\phi|} - \frac{D_\psi}{\psi}\nabla\psi. \tag{2.3}$$

The mass flux of the scalar ψ relative to the iso-surface is thus

$$\rho\psi \boldsymbol{u}_{\psi\phi} = \rho\psi \frac{\boldsymbol{n}(D\phi/Dt)}{|\nabla\phi|} - \rho D_\psi \nabla\psi. \tag{2.4}$$

The fine-grained surface density of the surface with $\phi = \varphi$ (Pope 1990; Vervisch *et al.* 1995) may be written in vector form as

$$\boldsymbol{\Sigma}_\varphi = \nabla\phi\,\delta(\phi - \varphi), \tag{2.5}$$

where $\delta(\phi - \varphi)$ is the Dirac delta function. $\boldsymbol{\Sigma}_\varphi$ is the fine-grained surface to volume ratio in vectorial form of the $\phi = \varphi$ surface with the orientation of the vector area in the same direction as for $\boldsymbol{n}$.

The fine-grained mass flow per unit volume of the scalar ψ, $\dot{m}'''_{\psi\varphi}$ is given by multiplying (2.4) by (2.5) to yield

$$\dot{m}'''_{\psi\varphi} = \left(\rho\psi \frac{\mathrm{D}\phi}{\mathrm{D}t} - \rho D_\psi \nabla\psi \cdot \nabla\phi\right) \delta(\phi - \varphi). \tag{2.6}$$

Ensemble averaging of (2.6) gives $R_{\psi\varphi}$, the average mass flow rate of the scalar ψ per unit volume through the iso-surface, $\phi = \varphi$, positive in the direction of increasing ϕ:

$$R_{\psi\varphi}(\boldsymbol{x}, t) = \left[\left\langle \rho\psi \frac{\mathrm{D}\phi}{\mathrm{D}t} | \phi(\boldsymbol{x}, t) = \varphi \right\rangle - \langle \rho D_\psi \nabla\psi \cdot \nabla\phi | \phi(\boldsymbol{x}, t) = \varphi \rangle\right] P(\varphi; \boldsymbol{x}, t), \tag{2.7}$$

where $P(\varphi; \boldsymbol{x}, t)$ is the probability density function (PDF) of ϕ at the point $(\boldsymbol{x}, t)$ for the ensemble. The terms involving angle brackets with a vertical bar denote ensemble averaging for the members of the ensemble in which the condition given to the right of the vertical bar is valid. Equation (2.7) is the general result that has been sought here. $R_{\psi\varphi}$ is called the '*iso-surface mass flow density*' of the scalar ψ through the iso-surfaces of ϕ with $\phi = \varphi$.

In the special case where ψ and ϕ are the same, we have

$$R_{\phi\varphi}(\boldsymbol{x}, t) = \left[\varphi \left\langle \rho \frac{\mathrm{D}\phi}{\mathrm{D}t} | \phi(\boldsymbol{x}, t) = \varphi \right\rangle - \langle \rho D_\phi \nabla\phi \cdot \nabla\phi | \phi(\boldsymbol{x}, t) = \varphi \rangle\right] P(\varphi; \boldsymbol{x}, t). \tag{2.8}$$

By setting $\psi = 1$ in (2.7), it can be seen that the average total mass flow rate of the fluid per unit volume through the iso-surface with $\phi = \varphi$ is given by

$$R_\varphi(\boldsymbol{x}, t) = \left\langle \rho \frac{\mathrm{D}\phi}{\mathrm{D}t} | \phi(\boldsymbol{x}, t) = \varphi \right\rangle P(\varphi; \boldsymbol{x}, t). \tag{2.9}$$

R_φ is called the '*iso-surface mass flow density*'. Equations (2.7)–(2.9) are new results that have important implications for turbulent mixing and combustion.

2.2. *Total mass flux across inhomogeneous layers*

In inhomogeneous flows, there will be strong spatial variations of the iso-surface mass flow density, $R_{\psi\varphi}$, which is, of course, a point-wise statistic. In such flows, interest is usually focused on the total mass flow across the iso-surface when this is integrated across the flow. The concepts of entrainment in free flows and of turbulent flame speed in turbulent premixed combustion are of this nature. In this subsection we formally define such crossflow total fluxes and relate them to the fundamental processes in the flow.

Figure 2 shows schematically the situation for some typical problems of interest. Here, the flow and mixing is statistically stationary and two-dimensional in nature,

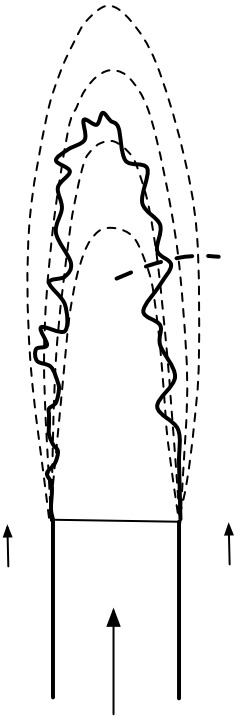

FIGURE 2. Schematic of a statistically stationary inhomogeneous turbulent flow such as a planar or round jet or a premixed flame on a slot burner or a Bunsen burner. Dashed curves denote iso-surfaces with the same value of the mean scalar $\widetilde{\phi}$. The full curve denotes an instantaneous iso-surface with $\phi = \varphi$. The bold dashed curve indicates the integration path used to obtain entrainment rate or turbulent flame speed.

either planar or axisymmetric. If it is jet mixing, the question of interest is the entrainment rate into the jet as a function of the threshold value, φ, of the scalar ϕ that is chosen. Integration across the layer along the path indicated is required. In practice, integration along the radius at a constant value of the axial coordinate may suffice. If the turbulent premixed flame burning velocity is of interest, integration of R_φ across the layer is required and it is likely to be dependent to a significant extent on the value chosen and perhaps also on the integration path. For axisymmetric cases, weighting of the integration by the radius is required. The fundamental analysis presented here has the potential of resolving these questions of classical importance in turbulent mixing and premixed flame propagation. The situation will be somewhat more complex in three-dimensional stationary flows and in flows that are not statistically stationary: the conceptual framework will not be fundamentally different, however.

The overall flux of the scalar ψ through the iso-ϕ surface can be obtained by integration of $R_{\psi\varphi}$ across an inhomogeneous layer. Consider a statistically one-dimensional planar layer. The integration of the surface mass flow density across the layer yields

$$\int_{-\infty}^{\infty} R_{\psi\varphi}\,\mathrm{d}x_1 = \left\langle \int_{-\infty}^{\infty} \rho\psi \boldsymbol{u}_{\psi\phi}\cdot\boldsymbol{n}|\nabla\phi|\delta(\phi-\varphi)\,\mathrm{d}x_1 \right\rangle = \left\langle \sum_i \left[\frac{\rho_\varphi \psi \boldsymbol{u}_{\psi\varphi}\cdot\boldsymbol{n}_\varphi}{|\boldsymbol{n}_\varphi\cdot\boldsymbol{e}_1|}\right]_i \right\rangle, \quad (2.10)$$

where $\boldsymbol{e}_1$ is the unit vector in the integration direction. The commutativity of integration and ensemble averaging is used in the first part of (2.10), while the second

part recognizes that for a single member of the ensemble, the integration path will only intersect the iso-surface a finite number of times and so can be expressed as a summation over these intersections. The term, $1/|\boldsymbol{n}_\varphi \cdot \boldsymbol{e}_1|$, is the ratio of the infinitesimal area of the iso-surface to its projected area onto the plane normal to the integration direction, which measures the increase of the area of the iso-surface owing to turbulent wrinkling. The term, $(\rho_\varphi \psi \boldsymbol{u}_{\psi\varphi} \cdot \boldsymbol{n}_\varphi)/|\boldsymbol{n}_\varphi \cdot \boldsymbol{e}_1|$, is the instantaneous mass flux of the scalar ψ across the iso-ϕ surface (per unit area of the plane normal to the integration direction). Therefore, the integration of the surface mass flow density $R_{\psi\varphi}$ across the inhomogeneous layer is the average total flux of the scalar ψ through the iso-surface with $\phi = \varphi$.

In general, the integration in (2.10) should take into account the overall geometry of the flow such as in axisymmetric and spherically symmetric flows, in order to conserve overall fluid mass, and hence the need for a weighting factor. The total scalar mass flux across an inhomogeneous layer can thus be written as

$$\Gamma_{\psi\varphi}(\boldsymbol{y}, t) = \int_{m_1}^{m_2} R_{\psi\varphi}(\boldsymbol{x}, t) w \, \mathrm{d}m, \tag{2.11}$$

where m is the coordinate along the integration path. The values m_1 and m_2 correspond, respectively, to $\widetilde{\phi}_{min}$ and $\widetilde{\phi}_{max}$, where $\widetilde{\phi}_{min}$ and $\widetilde{\phi}_{max}$ are the minimum and maximum of $\widetilde{\phi}$ along the integration line, respectively. $\widetilde{\phi}$ is the Favre mean of ϕ. Integration is performed along the path where the mean scalar evolves to include contributions from all iso-surfaces distributed over the integration path. It is assumed in (2.11) that $\widetilde{\phi}$ is monotonically increasing from $\widetilde{\phi}_{min}$ to $\widetilde{\phi}_{max}$ along the integration path. The coordinate $\boldsymbol{y}$ represents the location of the integration path, and w is a non-dimensional weighting factor. The weighting factor is equal to unity for the layers that are planar in the mean, r/r_r for axisymmetric layers and $(r/r_r)^2$ for spherically symmetric layers, where r_r is a suitably defined reference radius. Similarly, the total mass flux across an inhomogeneous layer can be evaluated as

$$\Gamma_{\varphi}(\boldsymbol{y}, t) = \int_{m_1}^{m_2} R_{\varphi}(\boldsymbol{x}, t) w \, \mathrm{d}m. \tag{2.12}$$

2.3. *Non-premixed combustion*

Theory of turbulent non-premixed combustion is well advanced (Bilger *et al.* 2005) and expressions have been derived for the reaction rate in the limit of fast chemistry. It should be possible to obtain these results using the present formula (2.7) for the iso-surface mass flow density in the fast chemistry case of a one-step irreversible reaction, where reaction occurs at a flame sheet. Such corroboration will support the validity of the iso-surface mass flow density theoretical results, and the improved understanding of the physics involved may also result. This is investigated in this subsection.

For non-premixed combustion, we choose ϕ as the mixture fraction ξ with a sample space variable $\varphi = \eta$ and ψ as a reactive species mass fraction Y. The mixture fraction ξ and the species mass fraction Y obey

$$\rho \frac{\mathrm{D}\xi}{\mathrm{D}t} = \nabla \cdot (\rho D_\xi \nabla \xi), \tag{2.13}$$

$$\rho \frac{\mathrm{D}Y}{\mathrm{D}t} = \nabla \cdot (\rho D_Y \nabla Y) + \omega_Y, \tag{2.14}$$

where Fickian diffusion is assumed with molecular diffusivities, D_ξ and D_Y for ξ and Y, respectively, and ω_Y is the chemical reaction rate of Y. Equation (2.7) may then be

written as

$$R_{Y\eta}(\boldsymbol{x},t)=\langle\rho Y\nabla\cdot(\rho D_\xi\nabla\xi)|\eta\rangle\,P(\eta;\boldsymbol{x},t)-\langle\rho D_Y\nabla Y\cdot\nabla\xi|\eta\rangle\,P(\eta;\boldsymbol{x},t). \tag{2.15}$$

Under fast chemistry conditions (Bilger 1976)

$$Y=Y^e(\xi), \tag{2.16}$$

equation (2.15) becomes

$$R_{Y\eta}=\rho_\eta Y^e(\eta)M_\eta P(\eta)-\left.\frac{\mathrm{d}Y^e}{\mathrm{d}\xi}\right|_\eta\rho_\eta N_\eta P(\eta). \tag{2.17}$$

Here, M_η is the conditional average diffusion defined as

$$M_\eta\equiv\frac{1}{\rho_\eta}\langle\nabla\cdot\left(\rho D_\xi\nabla\xi\right)|\xi=\eta\rangle. \tag{2.18}$$

The conditional average density and the conditional average scalar dissipation are, respectively, defined as

$$\rho_\eta\equiv\langle\rho|\xi=\eta\rangle, \tag{2.19}$$

$$N_\eta\equiv\frac{1}{\rho_\eta}\langle\rho D_\xi\nabla\xi\cdot\nabla\xi|\xi=\eta\rangle. \tag{2.20}$$

The $(\boldsymbol{x},t)$ dependence of these quantities and of the PDF are omitted to improve clarity. It has been assumed that $D_\xi=D_Y$.

If the reaction is one-step and irreversible then the function of (2.16) is piecewise linear (Bilger 1976) so that we have

$$\frac{\mathrm{d}Y^e}{\mathrm{d}\xi}=H(\xi_s-\xi)\left.\frac{\mathrm{d}Y^e}{\mathrm{d}\xi}\right|_-+H(\xi-\xi_s)\left.\frac{\mathrm{d}Y^e}{\mathrm{d}\xi}\right|_+ \tag{2.21}$$

with the gradients in mixture fraction space, $\mathrm{d}Y^e/\mathrm{d}\xi|_-$ and $\mathrm{d}Y^e/\mathrm{d}\xi|_+$, being invariant in their respective domains. There is thus a difference in $R_{Y\eta}$ on either side of the $\eta=\xi_s$ iso-surface, where ξ_s is the stoichiometric mixture fraction. This difference is

$$\Delta R_{Y\xi_s}=-\rho_\eta N_\eta P(\xi_s)\left[\left.\frac{\mathrm{d}Y^e}{\mathrm{d}\xi}\right|_+-\left.\frac{\mathrm{d}Y^e}{\mathrm{d}\xi}\right|_-\right] \tag{2.22}$$

with the conditional average density and scalar dissipation evaluated for $\eta=\xi_s$. This result can be shown to be equivalent to the average reaction rate per unit volume for the species Y given earlier (Bilger 1976). To do this we start with the result for the instantaneous reaction rate, ω_Y, for the general fast chemistry reaction of (2.16) of Bilger (1976)

$$\omega_Y=-\rho N\frac{\mathrm{d}^2Y^e}{\mathrm{d}\xi^2}. \tag{2.23}$$

For the fast irreversible one-step chemistry, (2.21) may be differentiated to yield

$$\frac{\mathrm{d}^2Y^2}{\mathrm{d}\xi^2}=\left[\left.\frac{\mathrm{d}Y^e}{\mathrm{d}\xi}\right|_+-\left.\frac{\mathrm{d}Y^e}{\mathrm{d}\xi}\right|_-\right]\delta(\xi-\xi_s). \tag{2.24}$$

Substituting this into (2.23) and taking the ensemble average yields

$$\langle\omega_Y\rangle=-\left[\left.\frac{\mathrm{d}Y^e}{\mathrm{d}\xi}\right|_+-\left.\frac{\mathrm{d}Y^e}{\mathrm{d}\xi}\right|_-\right]\langle\rho N\delta(\xi-\xi_s)\rangle=-\left[\left.\frac{\mathrm{d}Y^e}{\mathrm{d}\xi}\right|_+-\left.\frac{\mathrm{d}Y^e}{\mathrm{d}\xi}\right|_-\right]\rho_\eta N_\eta P(\xi_s). \tag{2.25}$$

Comparing (2.22) and (2.25), it is seen that the mean reaction rate is equal to the difference in the flow rate of the species across the reaction sheet, as is expected.

2.4. *Entrainment rate in scalar mixing*

The term 'entrainment' is used to denote the process that occurs across the interface between the turbulent and non-turbulent parts of a flow such as for a turbulent boundary layer or for jets, wakes and other free turbulent flows (Pope 2000). The concept is concerned with the introduction of vorticity fluctuations into the non-turbulent fluid. Non-vortical fluctuations can arise in the non-turbulent fluid owing to the action of pressure fluctuations. Vortical fluctuations can only come, however, from viscous diffusion from the turbulent part of the flow. It is traditional thinking that the rate of this entrainment is an absolute quantity that is not dependent on a threshold for the intensity of the vorticity fluctuations chosen to demarcate what is turbulent and what is non-turbulent fluid. In flows of this type, that involve a difference in the temperature or concentration of a fluid species between the turbulent and non-turbulent parts of the fluid, transfer of the scalar quantity across the interface between the turbulent and non-turbulent fluid can occur only by molecular conduction or diffusion. Contamination of the non-turbulent fluid by the scalar difference present in the turbulent fluid occurs by a process that is exactly analogous to that for vorticity fluctuations, certainly for cases where the Prandtl number or Schmidt number are close to unity. This similarity between scalar transport and vorticity fluctuation transport across the interface has led to the use of a scalar to define the boundary between the turbulent and non-turbulent fluid and to provide a measure of turbulence intermittency and its average, termed the intermittency factor (Pope 2000). In terms of the scalar, the entrainment rate can be defined as the total flux of uncontaminated fluid across an iso-surface having a small (threshold) value of the scalar. In traditional thinking, the entrainment rate should be independent of the threshold value chosen if it is small enough. Here we investigate such use of a scalar to evaluate the entrainment rate.

Equation (2.8) gives the average mass flow rate of the scalar per unit volume through the iso-surface with $\phi = \psi$. The average mass flow rate of the remaining fluid per unit volume through the iso-surface with $\phi = \psi$ is thus given by

$$\begin{aligned} R_{r\varphi} &= R_{\varphi} - R_{\phi\varphi} \\ &= (1-\varphi)R_{\varphi} + \langle \rho D_{\phi} \nabla\phi \cdot \nabla\phi | \phi = \varphi \rangle P(\varphi). \end{aligned} \tag{2.26}$$

With $\phi = \xi$, (2.26) may be written

$$R_{r\eta}(\boldsymbol{x}, t) = (1-\eta)\rho_{\eta} M_{\eta}(\boldsymbol{x}, t) P(\eta) + \rho_{\eta} N_{\eta} P(\eta). \tag{2.27}$$

The total mass flux of $(1-\xi)$ through the iso-ξ surfaces is given by

$$\Gamma_{r\eta}(\boldsymbol{y}, t) = \int_{m_1}^{m_2} [(1-\eta) M_{\eta}(\boldsymbol{x}, t) + N_{\eta}] \rho_{\eta} P(\eta) w \, \mathrm{d}m. \tag{2.28}$$

This is the required entrainment rate per unit area of an appropriately chosen mean position of the interface. In (2.28), η is the effective threshold chosen for the scalar. It can be noted that ρ_{η} is expected not to vary across the layer for low Mach numbers, except perhaps from the effects of differential diffusion. The mean surface density for the iso-surface with $\xi = \eta$ can be obtained by ensemble averaging the fine-grained surface denisty in scalar form:

$$\overline{\Sigma}_{\eta} = \overline{\boldsymbol{\Sigma}_{\eta} \cdot \boldsymbol{n}} = \langle |\nabla\xi| | \xi = \eta \rangle P(\eta). \tag{2.29}$$

The wrinkled surface area ratio is given by

$$A_\eta(\boldsymbol{y}, t) = \int_{m_1}^{m_2} \overline{\Sigma}_\eta w \, \mathrm{d}m = \int_{m_1}^{m_2} \langle |\nabla \xi| | \xi = \eta \rangle P(\eta) w \, \mathrm{d}m. \tag{2.30}$$

In turbulent jets and mixing layers, the quantity of interest is how much fluid is entrained in a unit distance of the main flow direction. The integration direction is then chosen to be perpendicular to the main flow direction. In the axisymmetric jet, for example, $\Gamma_{r\eta}$ is evaluated by integration of $R_{r\eta}$ along a radial direction, r, with the weighting factor of r/r_r. The entrainment is then measured by $\Gamma_{r\eta}$ for ξ values that are low compared to the mean mixture fraction on the centreline.

2.5. *Turbulent burning velocity in premixed combustion*

The definition of turbulent burning velocity in flows of complex geometry is a challenging problem in premixed combustion. In a Bunsen burner premixed turbulent flame and a V-shaped flame, the flame brush grows in width in the downstream direction. Because of the advective-time-developing nature of the flames, the mass flux normal to a mean flame surface, which is defined as an iso-surface of a mean scalar, can depend on the choice of the mean flame surface (Cheng & Ng 1984; Cheng & Shepherd 1991). In stagnating and counterflow flames with significant mean flow divergence, the mass flux normal to a mean planar leading edge does not give a meaningful value of turbulent flame speed because the incoming unburned mixture can leave without burning (Shepherd & Kostiuk 1994). The mass flux normal to a mean flame surface decreases from the unburned to the burned sides of the flame brush.

The reaction progress variable C in reaction front propagation is defined so as to obey the equation

$$\rho \frac{\mathrm{D}C}{\mathrm{D}t} = \nabla \cdot (\rho D_C \nabla C) + \rho \omega_C, \tag{2.31}$$

where ω_C is the reaction rate per unit mass and D_C is the molecular diffusivity for the progress variable. With $\phi = C$, we obtain

$$R_\zeta(\boldsymbol{x}, t) = (\rho_\zeta M_\zeta + \langle \rho \omega_C | \zeta \rangle) P(\zeta), \tag{2.32}$$

where ζ is the sample space variable for C. The conditional average density and the conditional average diffusion are defined, respectively, as

$$\rho_\zeta \equiv \langle \rho | \zeta = C \rangle, \tag{2.33}$$

$$M_\zeta \equiv \frac{1}{\rho_\zeta} \langle \nabla \cdot (\rho D_C \nabla C) | \zeta \rangle. \tag{2.34}$$

In premixed combustion, the surface mass flow density R_ζ measures the local consumption rate of fresh mixture through an iso-scalar surface. Note the contribution of the conditional diffusion term M_ζ. Equation (2.32) shows that the apparent burning rate, i.e. consumption rate of fresh mixture can depend on the value of ζ chosen. Integration of R_ζ across the flame brush gives the total mass flux through the iso-C surfaces:

$$\Gamma_\zeta(\boldsymbol{y}, t) = \int_{m_1}^{m_2} (\rho_\zeta M_\zeta + \langle \rho \omega_C | \zeta \rangle) P(\zeta) w \, \mathrm{d}m. \tag{2.35}$$

A turbulent burning velocity can be defined as

$$S_T(\zeta, \boldsymbol{y}, t) = \frac{\Gamma_\zeta(\boldsymbol{y}, t)}{\rho_u}, \tag{2.36}$$

where ρ_u is the unburnt density. The wrinkled surface ratio is given by

$$A_T(\zeta, \boldsymbol{y}, t) = \int_{m_1}^{m_2} \overline{\Sigma}_\zeta w \, \mathrm{d}m = \int_{m_1}^{m_2} \langle |\nabla C| | C = \zeta \rangle P(\zeta) w \, \mathrm{d}m. \tag{2.37}$$

In statistically one-dimensional planar turbulent premixed flames, the integration path is the direction normal to the mean flame brush, and the weighting factor w is unity. In spherically expanding flames, the integration is performed along the radial direction with the weighting factor of $(r/r_r)^2$. The turbulent flame speed S_T depends on the time t and the progress variable ζ in these flames. In flames of premixture round jets impinging and being stabilized on a flat plate, the integration can be performed along the normal to the flat plate. The turbulent flame speed S_T depends on the radial coordinate r and the progress variable ζ. In Bunsen burner flames and V-shaped flames, the surface mass flow density can be integrated along the normal to the mean contours of the reaction progress variable. In that case, the weighting factor can be evaluated from the mean-contour-based coordinate transform (Gouldin 1996).

In turbulent premixed flames, as an alternative to the progress variable, iso-surfaces of the density can be used to identify the flame fronts in the low-Mach-number limit. From the continuity equation we have

$$\frac{\mathrm{D}\rho}{\mathrm{D}t} = -\rho \nabla \cdot \boldsymbol{U}. \tag{2.38}$$

This yields

$$R_\kappa(\boldsymbol{x}, t) = -\langle \rho^2 \nabla \cdot \boldsymbol{U} | \kappa \rangle P_\rho(\kappa) = -\langle \nabla \cdot \boldsymbol{U} | \kappa \rangle \kappa^2 P_\rho(\kappa), \tag{2.39}$$

$$R_\nu = -R_\kappa = \langle \nabla \cdot \boldsymbol{U} | \nu \rangle P_v(\nu), \tag{2.40}$$

where κ is the sample space variable for ρ and $v = 1/\rho$ is the specific volume with sample space variable ν. Note that R_κ values will be negative for flows with positive dilatation, because positive values imply flow across the iso-surface in the direction of increasing ρ. It can be seen that for a premixed turbulent flame, the surface mass flow density is directly proportional to the conditional average dilatation. For uniform density propagating reaction fronts, the dilatation is zero but the PDF is a delta function. The conditional average dilatation has been shown to be important in the structure of turbulent premixed flames (Swaminathan *et al.* 1997). The total mass flux through the iso-v surface is given by

$$\Gamma_\nu(\boldsymbol{y}, t) = \int_{m_1}^{m_2} \langle \nabla \cdot \boldsymbol{U} | \kappa \rangle P_v(\nu) w \, \mathrm{d}m. \tag{2.41}$$

A turbulent burning velocity can be defined as in (2.36). This formulation can be more useful in some circumstances. For example, in experiments, it requires the measurements of the velocity and the density (temperature), whereas (2.36) requires the reaction rate, which can depend on all the species involved, as well as the temperature and the diffusivity. Equation (2.41) also implies a relationship between $\langle \nabla \cdot \boldsymbol{U} | \kappa \rangle$ and the diffusional and reactive terms at the kernel of the integral in (2.36).

3. Direct numerical simulations

Direct numerical simulations are carried out to demonstrate the usefulness of the proposed concepts in understanding iso-surface propagation in turbulent flows. The simulations are here confined to planar flows.

The fully compressible Navier–Stokes equations are solved:

$$\frac{\partial \rho}{\partial t} + \frac{\partial \rho u_j}{\partial x_j} = 0, \tag{3.1}$$

$$\frac{\partial \rho u_i}{\partial t} + \frac{\partial}{\partial x_j}(\rho u_i u_j) = -\frac{\partial p}{\partial x_i} + \frac{\partial \tau_{ij}}{\partial x_j} + \rho f_i, \tag{3.2}$$

$$\frac{\partial \rho e}{\partial t} + \frac{\partial}{\partial x_j}[(\rho e + p)u_j] = \frac{\partial u_k \tau_{jk}}{\partial x_j} + \frac{\partial}{\partial x_i}\left(\lambda \frac{\partial T}{\partial x_i}\right) + \rho Q \omega_\phi + \rho f_j u_j, \tag{3.3}$$

$$\frac{\partial \rho \phi}{\partial t} + \frac{\partial}{\partial x_j}(\rho u_j \phi) = \frac{\partial}{\partial x_j}\left(\rho D \frac{\partial \phi}{\partial x_j}\right) + \rho \omega_\phi, \tag{3.4}$$

where

$$\rho e = \frac{1}{2}\rho u_j u_j + \frac{p}{\gamma - 1}, \tag{3.5}$$

$$\tau_{ij} = \mu\left(\frac{\partial u_i}{\partial x_j} + \frac{\partial u_j}{\partial x_i} - \tfrac{2}{3}\delta_{ij}\frac{\partial u_k}{\partial x_k}\right), \tag{3.6}$$

p is pressure, e is the total internal energy (internal energy plus kinetic energy), ω_ϕ is the chemical reaction rate of the scalar ϕ, Q is a heat release parameter, and f_i is an external forcing term. The thermal conductivity λ and the diffusion coefficient D are given as

$$\lambda = \mu c_p / Pr, \quad D = \mu/(\rho Sc), \tag{3.7}$$

where c_p is the specific heat at constant pressure. The dynamic viscosity μ is given as

$$\mu = \mu_u (T/T_u)^n, \tag{3.8}$$

where $n = 0.7$. The Prandtl number, Pr, and the Schmidt number, Sc, are set to 0.7. The gas mixture is assumed to be a perfect gas with a specific heat ratio of $\gamma = 1.4$. The Mach number based on the root mean square (r.m.s.) velocity fluctuations is below 0.1 for all the cases studied here. The equations are integrated using a low storage fourth-order Runge–Kutta method with a sixth-order compact finite-difference scheme for spatial discretization (Kennedy, Carpenter & Lewis 2000; Lele 1992).

3.1. *Conserved scalar mixing*

Passive conserved scalar mixing in forced homogeneous isotropic turbulence is simulated: $\omega_\phi = 0$. Linear forcing of Lundgren (Lundgren 2003; Rosales & Meneveau 2005) is used:

$$f_i = A_f u_i, \tag{3.9}$$

where the forcing constant, A_f, is set to be 0.3 here. The Reynolds number based on Taylor microscale is 56. The passive conserved scalar field is periodic in the x_2 and x_3 directions, while the Dirichlet condition is used for the x_1 direction. The initial scalar profile is given by

$$\overline{\xi} = 0.5\,[1 + \mathrm{erf}(0.5(x_1 - x_{10})/\Delta_0)]\,, \tag{3.10}$$

where x_{10} is an origin for the x_1 coordinate and located at the centre of the domain. Δ_0 is set to be $0.01L$, where L is the characteristic length of the domain. Computation was continued until the boundary condition in the x_1-direction begins to influence the solution. The equations are solved on $256 \times 128 \times 128$ grid points.

	u'/s_L	l/l_F	Da	Ka	Re_λ
PF1	13.8	3.9	0.28	14	95
PF2	19.5	2.75	0.14	28	95

TABLE 1. Characteristics of the simulated premixed flames (u': r.m.s. initial turbulent velocity, l: initial integral length scale, S_L: laminar flame speed, l_F: flame thickness based on the maximum temperature gradient, $Da = S_L l/(u' l_F)$, $Ka = D_u^2/(S_L l_K)^2$, l_K: Kolmogorov length scale, D_u: unburned mixture diffusivity, Re_λ: Reynolds number based on the Taylor scale).

3.2. *Isothermal reaction fronts*

Reaction front propagation in homogeneous turbulence is simulated. The turbulence field is the same as that of the conserved scalar mixing case. The reaction rate is given by

$$\omega_c = A(1-C)\exp\left(-\frac{\beta}{\alpha C}\right), \tag{3.11}$$

where A is a pre-exponential factor. C is the reaction progress variable, $\alpha = 5$ and $\beta = 4$. The front is isothermal in the sense that $Q = 0$. The underlying flow field is the same as that for passive conserved scalar mixing. The whole flow and scalar fields are shifted after a few time steps to maintain the fronts in the centre of the computational domain. The scalar field is initialized using the laminar front solution with the front propagation speed S_L and the characteristic thickness l_F. The Damköhler number based on $u'/S_L = 17.67$ and $l/l_F = 3.3$ is 0.19, where u' and l are integral turbulence velocity and length scales, respectively.

3.3. *Premixed flames*

The simulated flames are statistically one-dimensional premixed flames propagating in decaying homogeneous turbulence. The reaction rate is given by

$$\omega_{Y_R} = AY_R \exp\left(-\frac{T_a}{T}\right), \tag{3.12}$$

where Y_R is the mass fraction of the deficient species in the reactant. The activation temperature T_a is set to be $4T_b$, where T_b is the burned gas temperature. The heat release parameter Q is chosen such that the density ratio between unburned and burned gas, γ, is equal to 6. The reaction progress variable is defined here as $C = 1 - Y_R$.

A non-reflecting boundary condition is used for the x_1-direction, while the x_2, and x_3, directions are periodic (Poinsot & Lele 1992). Although the non-reflecting boundary condition of Poinsot & Lele (1992) does not consider the chemical reactions at the boundaries, the flame fronts do not touch the non-reflecting boundaries in the present simulations. The equations are solved on $512 \times 256 \times 256$ grid points. Initial turbulence is homogeneous and isotropic. The characteristics of the premixed flames are shown in table 1. The initial turbulence intensity u'/s_L is larger than 10, while the length scale ratio l/l_F is about 3–4. The laminar flame thickness l_F is based on the maximum temperature gradient. The initial Damköhler numbers for cases PF1 and PF2 are 0.14 and 0.28, respectively. The velocity- and length-scale ratios are in the range of those in the previous studies (Trouve & Poinsot 1994; Kortschik, Plessing & Peters 2004; Chakraborty & Cant 2005; Thévenin 2005). Here the low Da regime where small-scale turbulence can disturb the flame fronts is of primary interest. The characteristics of iso-surfaces in this regime are not well understood as compared with those in the high Da flamelet regime.

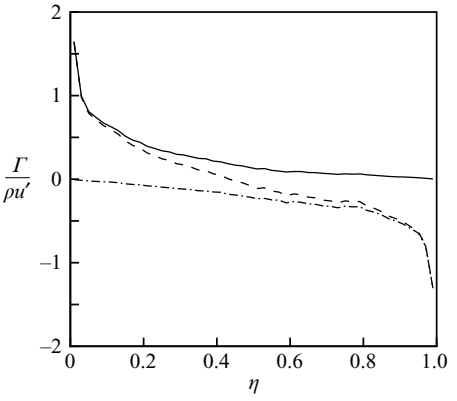

FIGURE 3. Entrainment rate, $\Gamma_{r\eta}$, in the scalar mixing layer as a function of the threshold η (solid line) at $\tau = 3.21$. Also shown are the total mass flow, Γ_{η}, through the η iso-surfaces (dashed line) and the flow, $\Gamma_{\xi\eta}$, of the mixture fraction ξ (dashed dotted line).

4. Results and discussion

In the present DNS database, the integration direction and the weight factor are $m = x_1$ and $w = 1$, respectively. The line integrated quantities, $\Gamma_{\psi\varphi}$ and Γ_{φ} for scalar fluxes and area ratio A_{φ}, have no dependence on the transverse spatial coordinates.

In this section, only a small selection of the possible range of statistically planar and one-dimensional flows are investigated. They have been chosen to illustrate the effects of time-dependence in scalar mixing, of considering reactive scalars rather than conserved scalars, and of the effect of heat release affecting both density and viscosity change. A more comprehensive investigation could include: the question of spatially varying but stationary conserved scalar mixing rather than the time-dependent case considered here; the effects of the form of the chemical kinetics used in the reacting flows; the influence of a wider range of *Da* in the reacting flows; separate treatment of the effects of heat release on density and viscosity change; and consideration of a range of heat release parameters. Such a broad investigation is required in order to gain a full understanding of the various factors that influence scalar mixing. This is beyond the scope of the present work. Rather, we show that the new iso-surface mass flow density formulation is a powerful tool that enables us to examine long-standing questions of the relative roles of iso-surface wrinkling and of iso-surface propagation speed in a series of closely related flows.

4.1. *Conserved scalar mixing*

For the time-developing planar mixing layer, figure 3 shows the entrainment rate $\Gamma_{r\eta}$ as a function of the threshold η at $\tau(=tl/u') = 3.21$. Also shown are the total scalar mass flux $\Gamma_{\xi\eta}$, and the total mass flux Γ_{η} through the iso-ξ surfaces. The negative of $\Gamma_{\xi\eta}$ is the entrainment rate of the scalar ξ. The entrainment rates, $\Gamma_{r\eta}$ and $-\Gamma_{\xi\eta}$, approach to Γ_{η} as η trends to the extreme values of the scalar. This indicates that the entrainment rate can be estimated with the total mass flux through the iso-ξ surface. The entrainment rate $\Gamma_{r\eta}$ shows sensitivity to the threshold value in figure 3, whereas the overall surface wrinkle ratio A_{η} does not show dependence on the scalar chosen in figure 4. The entrainment rate per unit area of the instantaneous iso-surface is, therefore, sensitive to the threshold value. This suggests that the entrainment rate is not a well-defined quantity in temporal mixing layers.

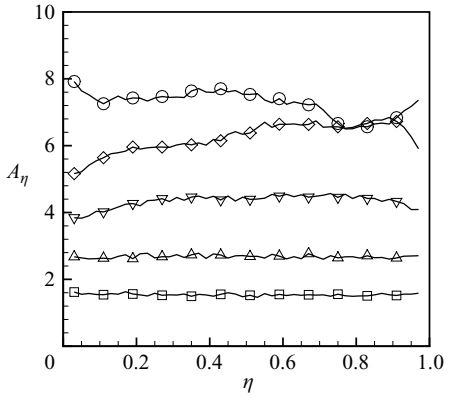

FIGURE 4. Wrinkled area ratio of the iso-η surfaces for conserved scalar mixing (squares, $\tau = 0.21$; triangles, $\tau = 0.54$; gradients, $\tau = 1.07$; diamonds, $\tau = 2.14$; circles, $\tau = 3.21$).

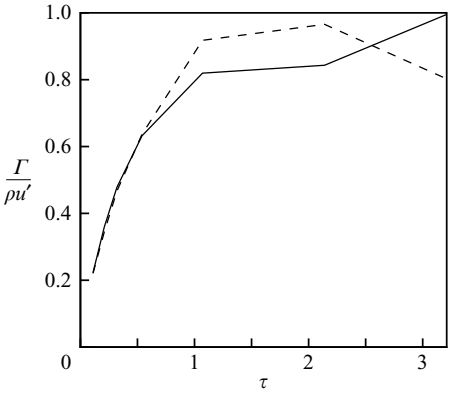

FIGURE 5. Time evolution of entrainment rates through the iso-η surfaces (solid line, $\Gamma_{r\eta_0}$; dashed line, $-\Gamma_{\xi\eta_1}$; $\eta_0 = 0.03$ and $\eta_1 = 0.97$).

In temporally growing self-similar scalar mixing layers, local diffusion layers are continuously growing. While the self-similarity is usually concerned with ensemble averages, it is expected that the norm of the scalar gradient averaged over the whole flow field with the condition that $\xi = \eta$, $\langle|\nabla\xi||\eta\rangle^*$, also shows the self-similarity in the scalar mixing layers. In constant density flows, the mass in the infinitesimal volume δV_η enclosed by the iso-surfaces with η and $\eta + \delta\eta$ can be estimated as $A_\eta \delta\eta / \langle|\nabla\xi||\eta\rangle^*$. Because the overall wrinkled surface ratio A_η is almost independent of η, the ratio of the fluid mass can be estimated as that of the conditional average scalar gradient $\langle|\nabla\xi||\eta\rangle^*$. Under these conditions, the ratio of fluid mass contained between $\eta - \delta\eta < \xi < \eta$ and that between $\eta < \xi < \eta + \delta\eta$ is time invariant. Therefore, the entrainment rate in the temporally growing mixing layers, which can be approximated by the total mass flux Γ_η for a small threshold value, increases as the threshold value η decreases. The sharp increase of the entrainment rate near the extremal values of the scalar may also have some implications for choosing the scalar threshold in the measurement of intermittency factor (Bilger *et al.* 1976).

Figure 5 shows the time evolution of entrainment rates, $\Gamma_{r\eta_0}$ and $-\Gamma_{\xi\eta_1}$, where $\eta_0 = 0.03$ and $\eta_1 = 0.97$. During the initial development, $\tau < 1$, $\Gamma_{r\eta_0}$ increases with time. The entrainment rate $\Gamma_{r\eta_0}$ then shows a weak dependence on time for $\tau > 1$. In

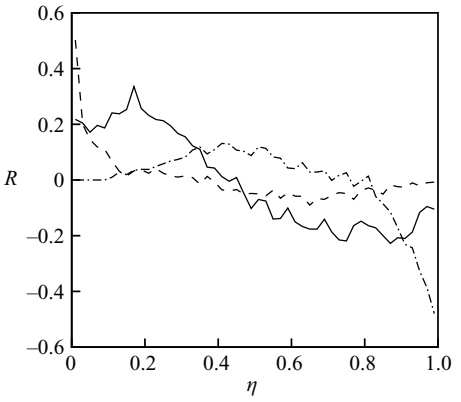

FIGURE 6. Surface mass flow density R_η at different locations in the scalar mixing layer (dashed line, $\overline{\xi} \approx 0.1$; solid line, $\overline{\xi} \approx 0.5$; dashed dotted line, $\overline{\xi} \approx 0.9$; normalized by $\rho u/l$; $\tau = 2.14$).

stationary homogeneous turbulence, the solution of the mean conserved scalar $\overline{\xi}$ can be written for $\tau > 1$ as

$$\overline{\xi} = 0.5\left[1 + \mathrm{erf}\left\{0.5(x_1 - x_{10})/(D_t t)^{1/2}\right\}\right], \tag{4.1}$$

where D_t is the turbulent diffusivity. This may be written as

$$x_1(\overline{\xi}, t) = x_{10} + 2\mathrm{erf}^{-1}(2\overline{\xi} - 1)(D_t t)^{1/2}. \tag{4.2}$$

The displacement speed of the iso-$\overline{\xi}$ surface is then given by

$$V_{\overline{\xi}} = \frac{\partial x_1}{\partial t} = \mathrm{erf}^{-1}(2\overline{\xi} - 1)\left(\frac{D_t}{t}\right)^{1/2} = \mathrm{erf}^{-1}(2\overline{\xi} - 1)u'\left(\frac{c_D}{\tau}\right)^{1/2}. \tag{4.3}$$

Here, $c_D \equiv D_t/(u'l)$. The entrainment rate through the iso-$\overline{\xi}$ surface is then given by

$$\begin{aligned} S_{\overline{\xi}} &= (1 - \overline{\xi})V_{\overline{\xi}} - D_t\frac{\partial(1 - \overline{\xi})}{\partial x_1} \\ &= \left[(1 - \overline{\xi})\mathrm{erf}^{-1}(2\overline{\xi} - 1) - \frac{1}{\sqrt{\pi}}\exp\left\{\frac{(x_1 - x_{10})^2}{4D_t t}\right\}\right]u'\left(\frac{c_D}{\tau}\right)^{1/2}. \end{aligned} \tag{4.4}$$

The entrainment rate through the iso-$\overline{\xi}$ surface thus scales with $\tau^{-1/2}$ for stationary homogeneous turbulence. The entrainment rate can be decomposed into the contribution from the increase of the wrinkled surface area ratio and that from the entrainment velocity. Initial increase of the entrainment rate in figure 5 is due primarily to the increase of the wrinkled surface area. The difference between the time dependence in figure 5 and that in (4.4) appears to arise from the fact that $\eta_0 = 0.03$ and $\eta_1 = 0.97$ are in the regions shown in figure 3 to be where the entrainment rate is very sensitive to η. It is likely that these are within the 'viscous superlayer' (Pope 2000). It seems that scaling with the turbulent diffusivity is not valid in the superlayer. It is apparent that this behaviour in the superlayer is worthy of further detailed investigation: this is beyond the scope of the present work.

Figure 6 shows the surface mass flow density R_η at different locations in the scalar mixing layer at $\tau = 2.14$. At the location with $\overline{\xi} \approx 0.1$, R_η is significant only for low values of η, $\eta < 0.2$, while it is slightly lower than zero for $\eta > 0.4$. At the opposite side of the layer, R_η is negative at high values of the scalar, $\eta \approx 1$. In general, R_η changes

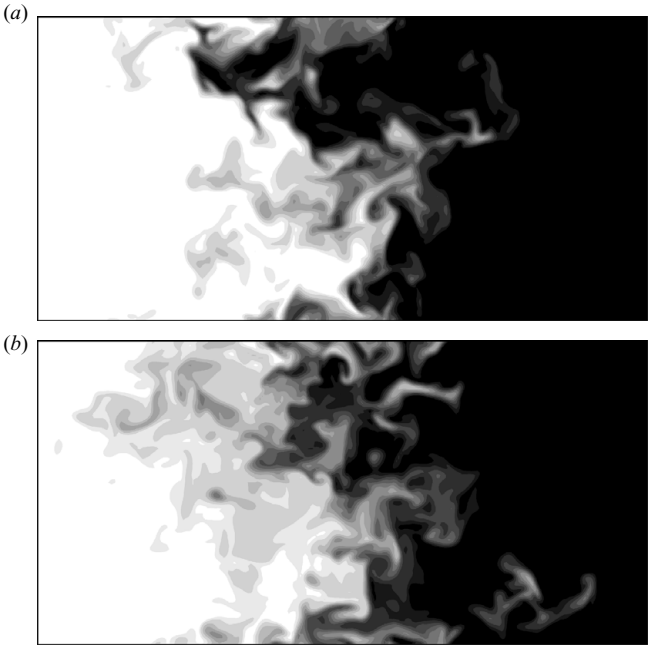

FIGURE 7. Instantaneous C-fields for isothermal reaction fronts at (*a*) $\tau = 3.2$ and (*b*) $\tau = 7.5$.

a sign at a scalar value which increases with the mean of the scalar. In the following subsection, it is shown that a similar behaviour of R_η is observed in reaction front propagation in a low Da regime.

4.2. *Isothermal reaction fronts*

Figures 7 (*a*) and 7 (*b*) show instantaneous fields of the progress variable, C, at $\tau = 3.2$ and $\tau = 7.5$, respectively. At $\tau = 3.2$, the thickness of fronts has a range of length scales. The relatively thin fronts have a smaller thickness than laminar fronts. The average thickness of the fronts is approximately equal to that of the laminar front at $\tau = 3.2$. At later time of $\tau = 7.5$, the fronts are much more thickened by small-scale turbulence. The mean progress variable at the inflow boundary is about 10^{-3} for $\tau > 6$.

Figure 8 shows the turbulent burning velocity, (2.36), defined for various iso-C surfaces at several time instants. Note that the turbulent burning velocity S_T is negative at high values of ζ at the early stage of $\tau = 1.7$. It then increases for all ranges of ζ until $\tau = 4.28$. The iso-surfaces for lower values of ζ propagate faster than those for higher values of ζ at $\tau < 4.28$. This implies that the reaction fronts are being thickened on average. In the stationary propagation stage, $\tau > 6$, S_T should be equal for all values of ζ, although the numerical results show some fluctuations. The thickness of the reaction front brush in the stationary propagation stage is $L/l_F \approx 29$, where L is the length of the domain with $0.05 < \overline{C} < 0.95$. $\overline{C}$ is the mean progress variable.

Figure 9 shows the average propagation speed of the iso-C surfaces relative to that for an unstretched laminar flame, $S_T/(A_T S_L)$. At $\tau = 1.07$, the average local propagation speed is much greater than the laminar value S_L for small values of ζ, whereas it is small and even negative for large values of ζ. During the transient stage of $2 < \tau < 5$, the front propagation speed is close to the laminar one in the reaction

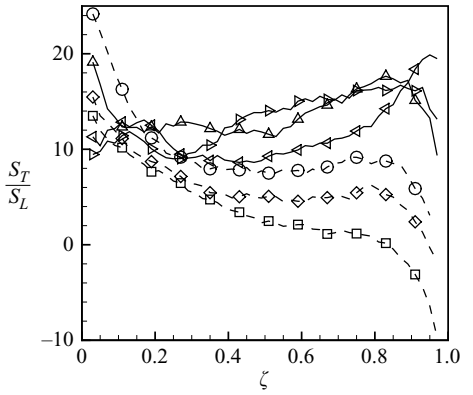

FIGURE 8. Turbulent burning velocity for isothermal reaction fronts (squares, $\tau = 1.07$; diamonds, $\tau = 2.14$; circles, $\tau = 4.28$; triangles, $\tau = 6.43$; right triangles, $\tau = 7.5$; left triangles, $\tau = 8.57$; solid lines denote the stationary state; dashed lines denote the transient state).

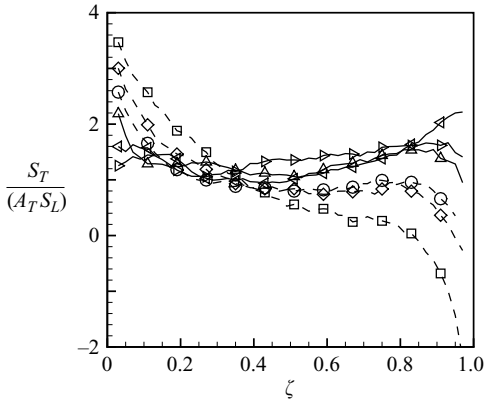

FIGURE 9. Average local propagation speed of the iso-C surfaces for isothermal reaction fronts (values as for figure 8).

zone. Iso-C surfaces for the pre-reaction zone propagate faster, whereas those for the post-reaction zone propagate more slowly than the laminar one during this period. In the stationary propagation stage, the propagation speed of iso-C surfaces is close to the laminar one for all values of ζ.

In the classical result of Damköhler (1940), the turbulent flame speed in the distributed reaction zone regime is given by $S_T/S_L \sim (D_t/D)^{1/2}$. An open question for this scaling law is whether the enhanced speed is due primarily to increased surface area or whether increased local propagation speed can also be significant. Bilger (2004) investigated the characteristics of the marker variable, which is introduced to mark the flame fronts, and found that the increase of the iso-surface area of the marker variable follows $(D_t/D)^{1/2}$ scaling. In this analysis, the stationary homogeneous field with uniform mean scalar gradient is assumed. Another key assumption is the Gaussian PDF of the scalar, for which the intermittency effects are not included. These assumptions are also relevant to the progress variable field in the distributed reaction zone regime. This suggests that $A_\zeta \sim (D_t/D)^{1/2}$ and that the average propagation speed of the iso-surface is of the order of the laminar front propagation speed as in

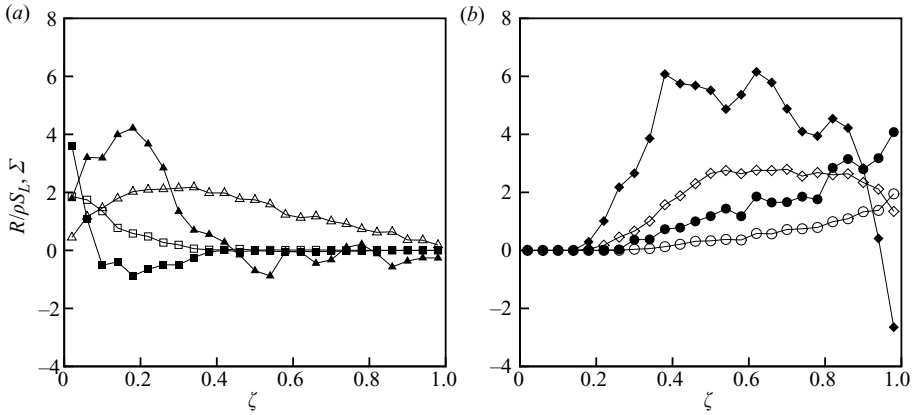

FIGURE 10. Surface mass flow density and surface density function for isothermal reaction fronts (filled symbols, $R_\zeta/(\rho S_L)$; empty symbols, $\overline{\Sigma}_\zeta$; squares, $\overline{C} \approx 0.05$; triangles, $\overline{C} \approx 0.3$; diamonds, $\overline{C} \approx 0.7$; circles, $\overline{C} \approx 0.95$; $\tau = 7.5$).

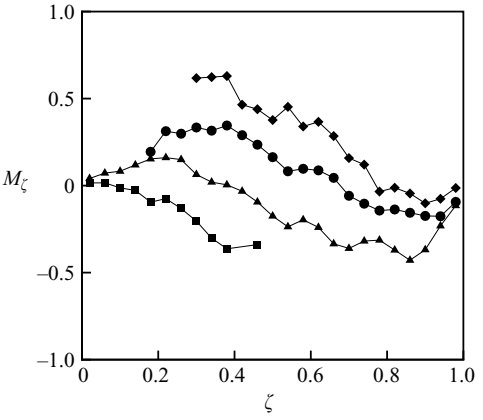

FIGURE 11. Conditional diffusion across the layer of isothermal reaction fronts (squares, $\overline{C} \approx 0.05$; triangles, $\overline{C} \approx 0.3$; circles, $\overline{C} \approx 0.7$; diamonds, $\overline{C} \approx 0.95$; $\tau = 7.5$).

figure 9. The question still remains about the effects of intermittency and finite *Da*, however.

Figure 10 shows the surface mass flow density R_ζ and the surface density function $\overline{\Sigma}_\zeta$ at $\tau \approx 7.5$. Local propagation characteristics are significantly different from those in the wrinkled laminar front propagation regime. In the location with $\overline{C}$ not being very close to 0 or 1, the local propagation velocity is higher than that of the laminar front for $\zeta < \zeta_0$, whereas it is lower than that of the laminar front for $\zeta > \zeta_0$. The value of ζ_0 increases with $\overline{C}$, which is similar to the behaviour observed in conserved scalar mixing in figure 6. At the trailing edge, iso-C surfaces propagate much faster than unstretched planar laminar fronts for the whole range of ζ. While the average propagation speed is close to the propagation speed of the laminar front, the local propagation property is significantly affected by turbulence in the low *Da* reaction fronts propagation.

The observed propagation characteristics of iso-scalar surfaces are related to the variation of the conditional diffusion M_ζ across the layer. In figure 11 the conditional

diffusion increases with increasing mean scalar. In the scalar field with the Gaussian PDF, the conditional diffusion is linear in the scalar space being zero at the value of the mean scalar (Pope & Ching 1993):

$$M_\varphi \sim \frac{1}{\tau_\phi}(\overline{\phi} - \varphi), \tag{4.5}$$

where τ_ϕ is the mixing time scale of the scalar ϕ. In scalar mixing layers and low *Da* reaction front propagation, the PDF is close to the Gaussian distribution except for the tails of the PDF and the boundaries of scalar space. The relationship of the PDF and the conditional diffusion for a general case (Pope & Ching 1993; Ching 1996) suggests that the linear relationship for the Gaussian PDF in (4.5) is a good first-order approximation of the conditional diffusion for this kind of PDF. The increase of the conditional diffusion with increasing mean scalar was also observed in simulations of spatially developing scalar mixing layers (de Bruyn Kops & Mortensen 2005).

The relation (4.5) and the results in figure 11 imply that the conditional diffusion in low *Da* turbulent reaction fronts is significantly different from that in laminar ones and primarily determined by the characteristics of the turbulent mixing field. According to (2.32), the mass flux through the iso-surfaces is governed by the balance of the conditional diffusion and the reaction rates. Since the conditional reaction rates are not affected by turbulence in the present case, the effects of turbulence on the propagation characteristics of iso-scalar surfaces are represented by the conditional diffusion. Negative burning velocity or propagation speed can occur for iso-surfaces with $C > \overline{C}$ when turbulent mixing is much stronger than chemical reactions. In the middle of the reaction front brush with low *Da*, the qualitative behaviour of the iso-surface propagation is explained well by the above argument based on the conditional diffusion for the scalar field where the PDF near the mean scalar is close to the Gaussian distribution. At the leading and trailing edges where the PDF is far from the Gaussian distribution, the propagation characteristics are different from those in the middle of the layer. At the trailing edge, iso-C surfaces propagate faster than unstretched planar laminar fronts for the whole range of ζ, while at the leading edge, iso-C surfaces propagate more slowly than unstretched planar laminar fronts for the whole range of ζ. These propagation characteritics at the leading and trailing edges are necessary to obtain statistically stationary propagation for which the turbulent burning velocity does not depend on ζ. It is expected that these behaviours are the characteristics of reaction front propagation in the low *Da* regime.

4.3. *Premixed flames*

Figure 12 shows the time evolution of the total burning rate, i.e. the integration of the mean reaction rate across the layer, normalized by $\rho_u S_L$. While the total burning rate is continuously growing, the growth rate decreases after $\tau \approx 2$, especially for PF2. The continuously growing total burning rate during the simulation of several eddy turnover times has been commonly observed in DNS of freely propagating premixed flames (Veynante & Poinsot 1997; Chakraborty & Cant 2005). The present simulation time is similar to or longer than the previous studies. Iso-C surfaces for the higher *Da* case PF1 and the lower *Da* case PF2 at $\tau \approx 4$ are shown in figures 13(*a*) and 13(*b*), respectively.

Figure 14 shows the surface mass flow density R_ζ and the surface density function $\overline{\Sigma}_\zeta$ for the cases PF1 and PF2. The surface density $\overline{\Sigma}_\zeta$ shows finite *Da* effects: it rapidly decreases with ζ near the leading edge, whereas it increases with ζ near the trailing edge. In the middle of the flame brush where most burning occurs, this

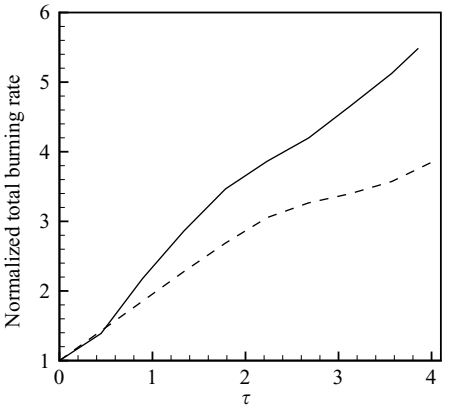

FIGURE 12. Time evolution of the total burning rate (solid line, PF1; dashed line, PF2; normalized by $\rho_u S_L$).

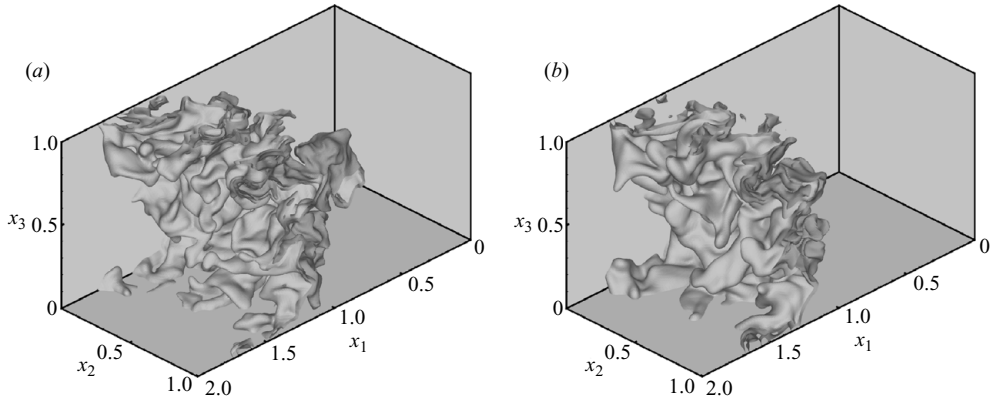

FIGURE 13. Iso-C surfaces for $C = 0.2$ and $C = 0.8$ in the premixed flames at $\tau \approx 4$ ($x_1 = 0$, unburned side; $x_1 = 2$, burned side). (*a*) PF1. (*b*) PF2.

dependence becomes weaker. For the iso-surface propagation speed, the departure from the laminar flamelet behaviour is weak as compared with that in the isothermal reaction fronts. This is probably due to the decay of the turbulence, the effects of increased viscosity in high temperature gas, and the dilatation in the reaction zone.

The surface density weighted average propagation speed, $R_\zeta/(\rho_u \overline{\Sigma}_\zeta)$, of iso-$C$ surfaces is compared with the conditional average of the displacement speed, $\langle \rho u_C | \zeta \rangle / \rho_u$, in figure 15. Although the two quantities are similar to each other, differences are observed at the leading and trailing edges. The difference between the two quantities comes from the correlation of the mass flux through the iso-surface and the fine grained surface density, $\langle \rho u'_C \Sigma'_\zeta | \zeta \rangle$. At the leading edge, this correlation is positive for $C < 0.4$.

While figure 14 gives point-wise statistics, in figure 16, we show similar information integrated across the layer: the turbulent burning velocity defined for various iso-C surfaces, S_T, and the total wrinkled area, A_T. The turbulent burning velocity S_T and the total wrinkled area A_T show a dependence on ζ. For PF1, the turbulent burning rate normalized by the laminar one, S_T/S_L, is larger than A_T for $\zeta < 0.5$, which indicates that iso-C surfaces for low values of ζ propagate faster than the

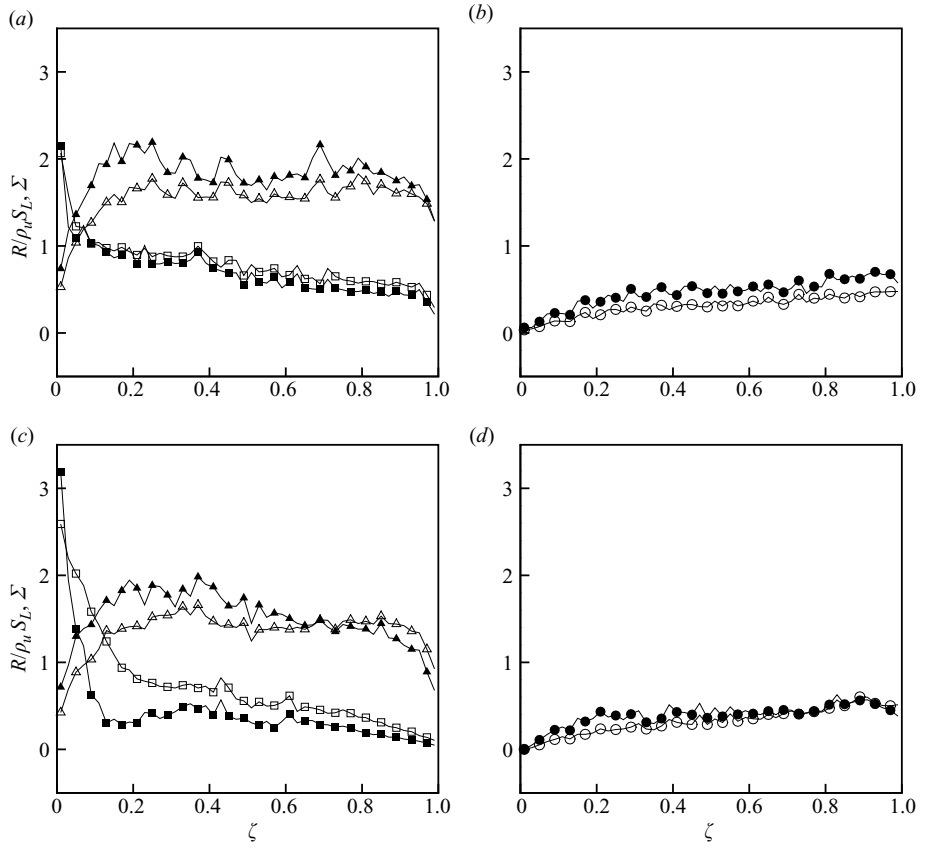

FIGURE 14. Surface mass flow density and surface density function for the premixed flames (filled symbols, $R_\zeta/(\rho_u S_L)$; open symbols, $\overline{\Sigma}_\zeta$; squares, $\widetilde{C}=0.03$; triangles, $\widetilde{C}=0.4$; circles, $\widetilde{C}=0.9$; $\tau\approx 4$). (*a*, *b*) PF1. (*c*, *d*) PF2.

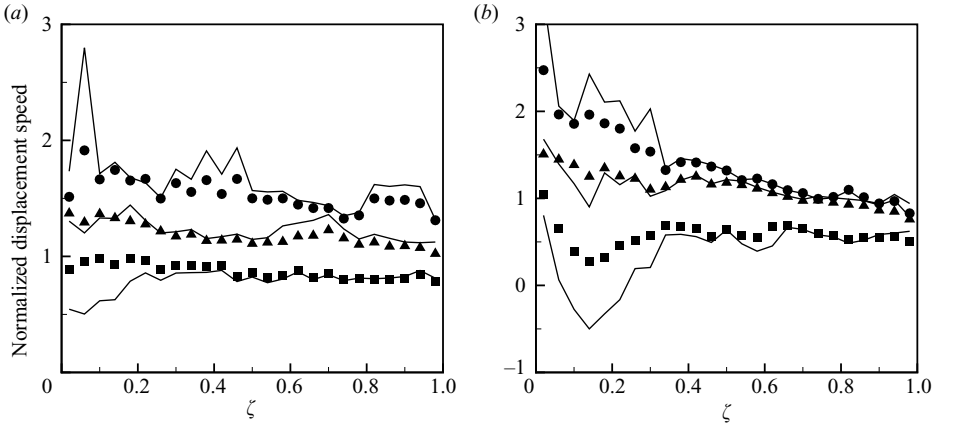

FIGURE 15. Comparison of the surface density weighted propagation speed, $R_\zeta/(\rho_u S_L\overline{\Sigma}_\zeta)$, (symbols) and the conditional average of the displacement speed, $\langle \rho u_C|\zeta\rangle/(\rho_u S_L)$, (lines) at $\tau\approx 4$ (squares, $\widetilde{C}=0.03$; triangles, $\widetilde{C}=0.4$; circles, $\widetilde{C}=0.9$). (*a*) PF1. (*b*) PF2.

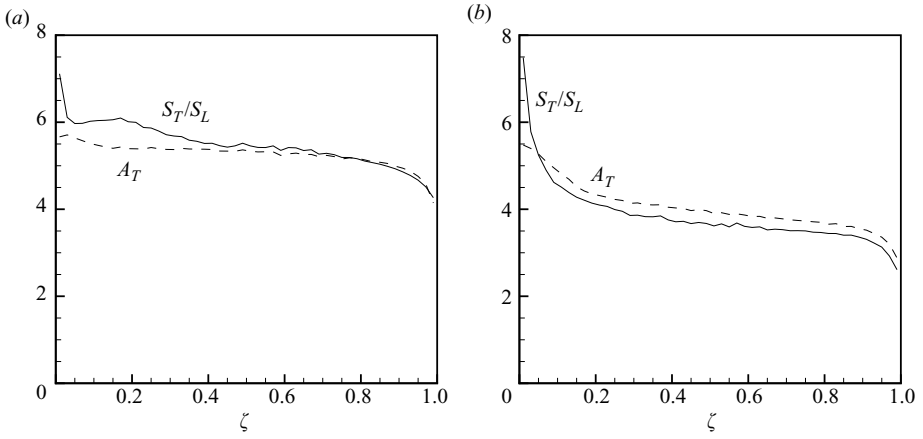

FIGURE 16. Turbulent burning velocity and wrinkled surface area ratio for the premixed flames at $\tau \approx 4$. (*a*) PF1. (*b*) PF2.

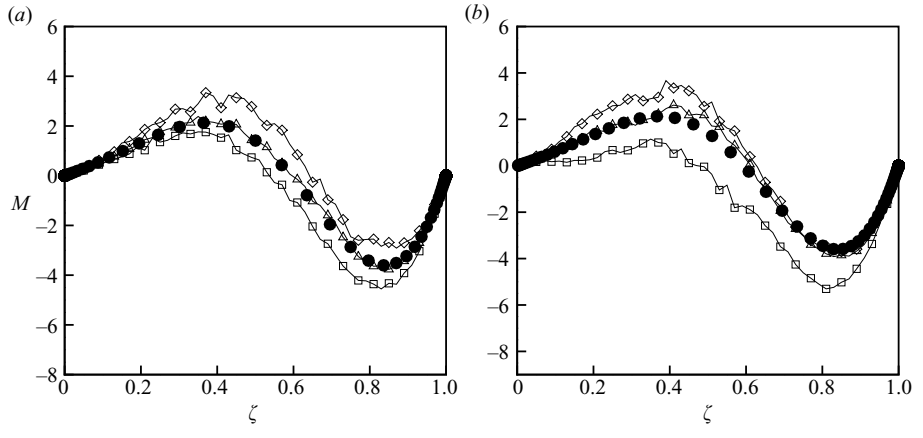

FIGURE 17. Conditional diffusion (circles, laminar value; squares, $\widetilde{C} = 0.03$; triangles, $\widetilde{C} = 0.4$; diamonds, $\widetilde{C} = 0.9$; normalized by l_F/S_L; $\tau \approx 4$). (*a*) PF1. (*b*) PF2.

laminar flame on average. However, the propagation characteristics generally follow the wrinkled laminar flame propagation. For PF2, S_T/S_L is higher than A_T for $\zeta < 0.1$, whereas it is lower than A_T for $\zeta > 0.1$. The time required to achieve a steady state increases as *Da* decreases. In figure 16, wrinkling of the iso-surfaces is highest for low values of ζ and significantly lower for high values of ζ, particularly for the lower *Da* case PF2. This supports the concept of the 'thin reaction zone' regime of flame structure where the turbulence increases wrinkling in the preheat zone. Wrinkling is also decreased in the burnout zone of the front, perhaps owing to the effect of high viscosity dampening the turbulence.

For turbulent premixed flames that are in the wrinkled laminar flamelet regime, the structure of the local flame front is close to that in an unstretched planar laminar flame. For significant amounts of wrinkling, the radius of curvature of the flame front can become of the same order as the thickness of the instantaneous flame front. For the current chemistry with Lewis numbers unity, these effects must come from the conditional diffusion M_ζ, (figure 17). The dependence of M_ζ on the locations of the flame brush in figure 17 is primarily due to these curvature effects and is also consistent with

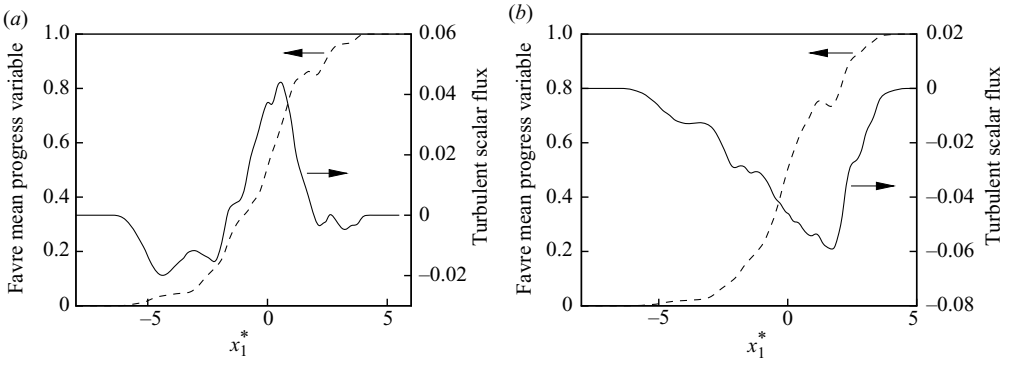

FIGURE 18. Distributions of the Favre mean and turbulent flux of the progress variable (solid line, turbulent scalar flux normalized by u'; dashed line, the Favre mean progress variable; $x_1^* = (x_1 - x_0)/l$ where x_0 represents the centre of the flame brush; $\tau \approx 4$). (*a*) PF1. (*b*) PF2.

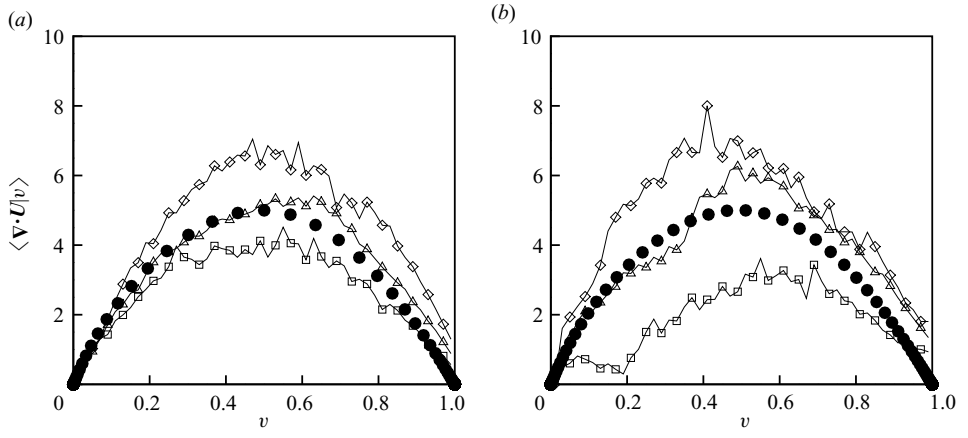

FIGURE 19. Conditional dilatation (circles, laminar value; squares, $\widetilde{C} = 0.03$; triangles, $\widetilde{C} = 0.4$; diamonds, $\widetilde{C} = 0.9$; normalized by l_F/S_L; $\tau \approx 4$). (*a*) PF1. (*b*) PF2.

the previous observation for the isothermal reaction fronts with low *Da*. For the low *Da* case, PF2, turbulent premixed flames have more significant effects of small-scale turbulence on the structure of the instantaneous flame front near the leading edge. The form and values of M_ζ are influenced by small-scale turbulence in figure 17(*b*), but not as significantly as in the isothermal reaction front problem. The turbulent burning velocity can depend on the choice of ζ in these cases. The effects of the curvature and the small-scale turbulence are more evident near the leading and trailing edges.

Figure 18 shows the distributions of the Favre mean progress variable $\widetilde{C}$ and the turbulent scalar flux $\widetilde{c''u_1''}$ for the cases PF1 and PF2, where the double prime denotes fluctuations about the Favre mean. For the higher *Da* case PF1, turbulent scalar fluxes are in the counter-gradient direction in the middle of the flame brush, whereas they are in the gradient direction at the leading and trailing edges. As *Da* decreases, countergradient diffusion is not observed for the whole region of the flame brush in figure 18(*b*).

Figure 19 shows the conditional dilatation for the cases PF1 and PF2. The conditional dilatation varies from the unburnt to the burnt side. The shape of the

conditional dilation is significantly different from that of the unstretched laminar flame at the leading edge for the lower Da case PF2. Although not shown, for the location where $\widetilde{C} < 0.02$, the peak moves to the unburnt side of the local flame fronts, which is favourable to transition to the gradient transport of the scalar flux (Swaminathan *et al.* 1997).

In statistically one-dimensional steady premixed flames, turbulent scalar fluxes have a close relationship with the local flame structure (Swaminathan *et al.* 1997). Using the concept of the surface mass flow density, this relation can be written as

$$\begin{aligned}\int_{-\infty}^{\infty} \widetilde{\bar{\rho} u_1'' c''} \frac{\mathrm{d}\widetilde{C}}{\mathrm{d}x_1}\,\mathrm{d}x_1 &= \frac{\rho_u}{\gamma-1}\int_{-\infty}^{\infty}\int_0^1 (\zeta-\widetilde{C}) R_\zeta\,\mathrm{d}\zeta\,\mathrm{d}x_1 \\ &= \frac{\rho_u}{\gamma-1}\left(\tfrac{1}{2}S_T - \int_{-\infty}^{\infty}\widetilde{C}\int_0^1 R_\zeta\,\mathrm{d}\zeta\,\mathrm{d}x_1\right). \end{aligned} \tag{4.6}$$

This shows the relationship between the local propagation property and the mean scalar transport. According to the results in figures 10 and 14, variations of the local propagation speed owing to departure from the unstretched laminar flamelet structure increase the tendency to gradient diffusion, especially at the leading edge.

While conserved scalar mixing can be considered as the zero Da case, for which the diffusion layers are continuously broadened for thin enough initial layer thickness, it does not describe behaviour in the limiting case of $Da \to 0$ and $t \to \infty$. When the initial planar laminar fronts are subject to strong turbulence, i.e. in low Da limit, the initial increase of the reactant consumption speed is primarily determined by turbulent transport. The initial propagation characteristics of the iso-surfaces of the progress variable is then similar to that of the conserved scalar. During the transient period, the brush thickness increases, while the scalar gradients in the brush decrease. A stationary state is reached when the steepening of scalar gradients by chemical reactions is balanced with mitigation of scalar gradients as a result of turbulent mixing. In the KPP theory (Kolmogorov, Petrovskii & Piskunov 1937; Lipatnikov & Chomiak 2005), the diffusion–reaction equation has an asymptotic propagating solution at $t \to \infty$ with some restrictions on the reaction rate. The KPP result is for a constant positive (here turbulent) diffusivity. In the present isothermal reaction fronts with low Da, the turbulent diffusivity is positive throughout the layer, and a stationary state is reached at large τ in agreement with the KPP theory.

In premixed flames with heat release, there is a question about the turbulent diffusivity. At high Da, we have countergradient flux and so a negative turbulent diffusivity. Bray (1991) contended that the flux is the gradient at the unburnt edge of the flame and so that a stationary flame is found at high Da. On the other hand, Zimont (1979) claimed that the layer never becomes stationary even at low Da. Assuming that there exists a regime where turbulent scalar fluxes are in a countergradient direction for the whole field under the given mean pressure gradient and flow geometry, there exists a critical Damköhler number Da_{C1} just below which the change of sign of the turbulent scalar flux occurs. The DNS data support Bray's argument that this sign change begins to occur at the leading edge. The present analysis shows that this is related to the fact that turbulence more effectively increases the propagation speed of iso-C surfaces for low values of C at the leading edge. There also should be the Damköhler number $Da_{C2}(< Da_{C1})$ below which the turbulent scalar fluxes are in a gradient direction for the whole field. Based on the KPP theory and the above discussion, a steady planar premixed flame exists when $Da < Da_{C2}$. Bray (1991) contended that the steady planar flame is found even at $Da = Da_{C1} = \infty$. While a

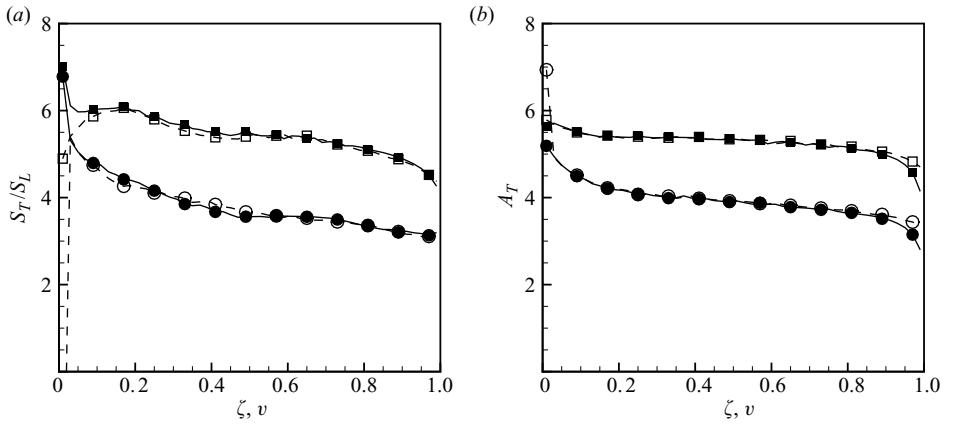

FIGURE 20. Comparison of (*a*) turbulent burning velocity and (*b*) wrinkled surface area ratio based on the reaction progress variable and those based on the specific volume in PF1 (filled symbols, reaction progress variable based quantity; open symbols, specific volume based quantity; circles, $\tau \approx 2.2$; squares, $\tau \approx 4$).

stationary state can be reached in low *Da* flames, the existence of the stationary state for high *Da* flames is still an open problem.

Figure 20 (*a*) compares turbulent burning velocity based on the progress variable $S_T(\zeta)$ and that based on the specific volume $S_T(v)$ at $\tau \approx 2.2$ and 4 in PF1. $S_T(\zeta)$ and $S_T(v)$ are in good agreement for ζ and $v > 0.1$. The difference for very low values of ζ and v is due to compressibility effects in finite-Mach-number flows. Wrinkled surface area ratio based on the progress variable $A_T(\zeta)$ also compares well with that based on the specific volume $A_T(v)$ in figure 20 (*b*).

4.4. *General discussion*

For the cases studied here, there appears to be no consistent pattern for the relative roles of iso-surface wrinkling and iso-surface propagation in scalar mixing. For the temporal scalar mixing layer, mixing at low values of η comes from increased speed of iso-surface propagation. For the iso-thermal reaction front studied, a stationary state is reached in which there is little effect of ζ on the amount of wrinkling or on the propagation velocity for quantities integrated across the layer: within the layer, however, the point-wise statistics show behaviour that is much more complex than expected for a wrinkled laminar propagating front. For the premixed flames studied, however, the structure is close to that for wrinkled laminar flames, both for point-wise statistics within the layer and for quantities integrated across the layer. The lower *Da* results indicate increased wrinkling in the preheat zone of the instantaneous flame-front and decreased wrinkling in the reaction completion or burnout zone.

As indicated at the beginning of this section, a more comprehensive series of cases must be investigated to ascertain the relative effects of temporal development, scalar reactivity and heat release on the relative roles of iso-surface wrinkling and iso-surface propagation in scalar mixing.

5. Discussion on turbulent burning velocity

The fine-grained mass flow rate $\dot{m}'''_C$ in (2.6) measures the mass flow rate normal to a iso-*C* surface for a single measurement. Considering a stationary oblique (planar) laminar flame, the ensemble average of $\dot{m}'''_C$ is the same as a value for the single

measurement. It can be shown in the laminar flame that the integration of the surface mass flow density along the flame normal coordinate n yields the mass flux normal to the flame surface:

$$\int_{-\infty}^{\infty} -\rho u_C |\nabla C| \delta(C-\zeta)\,\mathrm{d}n = -\rho_\zeta u_\zeta. \tag{5.1}$$

This gives the laminar flame speed $(-\rho_\zeta u_\zeta)/\rho_u$. In turbulent flames, these surfaces fluctuate in the flame brush. The surface mass flow density is a measure of the local mass flux. Fluctuations of the iso-scalar surface in the flame brush are considered by integration across the flame brush. In analogy with the laminar flame, integration can be performed along the normal to the contour of the mean progress variable.

A key feature of the surface mass flow density and the total mass flux across the inhomogeneous layer proposed here is that they are based on conditional averaging of the mass flux across an instantaneous iso-surface. Gouldin (1996) suggested a burning rate integral to measure the intensity of burning in laminar and turbulent flames. It is a generalization of the method by Shepherd & Kostiuk (1994), which was devised to consider a divergent flow in the counterflow and impinging flames. A similar integration to the present approach was adopted, but with the mean reaction rate as a kernel of the integral. Assuming a steady state, the burning rate integral was related to quantities from velocity and density fields, as in (2.41). The definition of turbulent burning velocity in non-stationary developing flames was considered by Lipatnikov & Chomiak (2002). Their method is based on the propagation of a mean flame brush or iso-surfaces of the mean scalar. It contains turbulent fluctuation effects inside the flame brush: for $\overline{C} \approx 0.5$, the burned and unburned mixtures present with equal probability in high Da flames. The non-stationary effects in their argument are, therefore, primarily due to growing flame brush by large-scale wrinkling. On the other hand, in the present definition of turbulent burning velocity, the dependence of turbulent flame speed on ζ comes from local flame fronts disturbed by turbulence. The non-stationary effects due to the large-scale wrinkling do not directly influence the ζ-dependence in the present method.

In general, the turbulent burning velocity S_T depends on the value of ζ as well as on the location of the integration path. If the flame brush is statistically stationary, planar and one-dimensional, the turbulent burning velocity does not depend on the value of ζ chosen. This single value of the turbulent burning velocity is the same as the mean fluid velocity in the cold boundary in that case. During the developing phase of the one-dimensional flame, S_T shows dependence on ζ when the local flame fronts are disturbed by turbulence. In practical flames and most laboratory flames, there is divergence in the flow, and the turbulent burning velocity can depend on the value chosen for ζ. In Bunsen flames and V-shaped flames, the anchoring of these flames at a particular location is analogous to the initial conditions of the planar flames studied here. Time development of the layer in the planar case is analogous to advection downstream in these anchored flames. Usually, there will be insufficient advective time to reach a steady state so that the flame speed will depend on ζ.

6. Conclusions

A new result has been derived for the mass flow rate per unit volume through a scalar iso-surface (the iso-surface mass flow density). The expressions of the entrainment velocity for scalar mixing and turbulent burning velocity for premixed combustion are obtained by integrating this quantity in the direction of mean scalar

inhomogeneity. In contrast to the previous ones, the proposed expressions are based on conditional averaging on an instantaneous iso-scalar surface and consider the dependence on a value of the scalar chosen. For non-premixed turbulent reacting flow, it is verified that this new result is consistent with the classical result of Bilger (1976) for fast one-step irreversible chemical reactions.

Direct numerical simulation data for conserved scalar mixing and reaction front propagation in stationary homogeneous turbulence and one-dimensional turbulent premixed flames are analysed using the proposed method. In the conserved scalar mixing case, the issue of the dependence of the entrainment velocity on a threshold value of the scalar is addressed. Results show that the entrainment velocity is sensitive to a threshold value, while the wrinkled surface ratio is almost constant for the whole range of the scalar value. This suggests that the entrainment velocity is not a well-defined quantity in temporally developing mixing layers. Furthermore, it appears that scaling in the viscous superlayers is anomalous and warrants further investigation.

In the reaction front propagation problems, the effects of small-scale turbulence and non-stationarity on the turbulent burning velocity are addressed. It is shown in the isothermal reaction front problem that small-scale turbulence enhances the local propagation speed for the iso-surfaces with lower values of the reaction progress variable, whereas it decreases the local propagation speed of the iso-surfaces with higher values of the reaction progress variable, except for the leading and trailing edges. The value of the progress variable for which this transition occurs increases with the mean progress variable. These characteristics of the reaction front with low Da are observed in point-wise statistics, while the propagation speed integrated over the inhomogeneous layer is close to an unstretched laminar front value. These observations are discussed in terms of the characteristics of the conditional diffusion and the scaling of the turbulent burning velocity and the wrinkled surface ratio in that regime.

In the premixed flames, the propagation characteristics are found to be close to those of the quasi-laminar flame propagation, perhaps owing to the decay of the turbulence in the whole flow field, and the effects of high viscosity and dilatation dampening the turbulence. Wrinkling of the iso-surfaces is highest for low values of the progress variable and significantly lower for high values of the progress variable, particularly for the lower Da flame studied here. This supports the concept of the 'thin reaction zone' regime of the flame structure where the turbulence increases wrinkling in the preheat zone. During the developing phase of the present flames, the turbulent burning velocity is shown to be higher for lower values of the reaction progress variable. Increased overall propagation speed at lower values of the progress variable comes less from iso-surface wrinkling and more from increased propagation of the instantaneous iso-surface.

In the present method, the non-stationarity effects and the dependence of the turbulent burning velocity on the value of the progress variable are due to flame fronts disturbed by turbulence and are not influenced by large-scale wrinkling. Time development of the layer in the present planar flames is analogous to advection downstream in anchored flames such as Bunsen flames and V-shaped flames. It is also shown that the propagation characteristics represented by the surface mass flow density and the turbulent burning velocity have a close relationship with the turbulent scalar flux in a statistically stationary one-dimensional premixed flame. Variations of the local propagation characteristics due to departure from the unstrained laminar flamelet structure are shown to decrease the tendency to countergradient transport in turbulent premixed flames.

The authors would like to thank Dr Nondas Mastorakos for helpful suggestions. The first author acknowledges the support of the US department of Energy within the ASC program. In Australia this work is supported by the Australian Research Council. R. W. B. also acknowledges the support of the Abdus Salam International Centre for Theoretical Physics, Trieste, Italy, where the basic ideas for the analysis were developed during a visit in 2004.

REFERENCES

Bilger, R. W. 1976 The structure of diffusion flames. *Combust. Sci. Technol.* **13**, 155–170.

Bilger, R. W. 2004 Marker fields for turbulent premixed combustion. *Combust. Flame* **138**, 188–194.

Bilger, R. W., Antonia, R. A. & Srinivasan, K. R. 1976 The determination of intermittency from the probability density function of a passive scalar. *Phys. Fluids* **19**, 1471.

Bilger, R. W., Pope, S. B., Bray, K. N. C. & Driscoll, J. M. 2005 Paradigms in turbulent combustion research. *Proc. Combust. Inst.* **30**, 21–42.

Bray, K. N. C. 1991 Studies of the turbulent burning velocity. *Proc. R. Soc. Lond.* A **431**, 315–335.

de Bruyn Kops, S. M. & Mortensen, M. 2005 Conditional mixing statistics in a self-similar scalar mixing layer. *Phys. Fluids* **17**, 095107.

Candel, S. M. & Poinsot, T. J. 1990 Flame stretch and the balance equation for flame area. *Combust. Sci. Technol.* **70**, 1–15.

Chakraborty, N. & Cant, R. S. 2005 Influence of Lewis number on curvature effects in turbulent premixed flame propagation in the thin reaction zones regime. *Phys. Fluids* **17**, 105105.

Cheng, R. K. & Ng, T. T. 1984 On defining the turbulent burning velocity in premixed V-shaped turbulent flames. *Combust. Flame* **57**, 155–167.

Cheng, R. K. & Shepherd, I. G. 1991 The influence of burner geometry on premixed turbulent flame propagation. *Combust. Flame* **85**, 7–26.

Ching, E. C. S. 1996 General formula for stationary or statistically homogeneous probability density functions. *Phys. Rev.* E **53**, 5899–5903.

Damköhler, G. 1940 Der einflußder Turbulenz auf die Flammengeschwidigkeit in Gasgemischen. *Z. Electrochem.* **46**, 601–652.

Gibson, C. H. 1968 Fine structure of scalar fields mixed by turbulence. I. Zero-gradient points and minimal gradient surfaces. *Phys. Fluids* **11**, 2305–2315.

de Goey, L. P. H. & Boonkkamp, J. H. M. 1999 A flamelet description of premixed laminar flames and the relation with flame stretch. *Combust. Flame* **119**, 253–271.

Gouldin, F. C. 1996 Combustion intensity and buring rate integral of premixed flames. *Proc. Combust. Inst.* **26**, 381–388.

Kennedy, C. A., Carpenter, M. H. & Lewis, R. M. 2000 Low-storage, explicit Runge–Kutta schemes for the compressible Navier–Stokes equations. *Appl. Numer. Maths.* **35**, 177–219.

Klimenko, A. Y. & Bilger, R. W. 1999 Conditional moment closure for turbulent combustion. *Prog. Energy Combust. Sci.* **25**, 595–687.

Kolmogorov, A. N., Petrovskii, I. G. & Piskunov, N. S. 1937 A study of the diffusion equation with a source term for application to a biological problem. *Bull. Moscow State Univ.* A **1**, 1.

Kortschik, C., Plessing, T. & Peters, N. 2004 Laser optical investigation of turbulent transport of temperature ahead of the preheat zone in a premixed flame. *Combust. Flame* **236**, 43–50.

Lele, S. K. 1992 Compact finite difference schemes with spectral-like resolution. *J. Comput. Phys.* **103**, 16–42.

Lipatnikov, A. N. & Chomiak, J. 2002 Turbulent burning velocity and speed of developing, curved, and strained flames. *Proc. Combust. Inst.* **29**, 2113–2121.

Lipatnikov, A. N. & Chomiak, J. 2005 Self-similarly developing, premixed, turbulent flames: A theoretical study. *Phys. Fluids* **17**, 065105.

Lundgren, T. 2003 Linearly forced isotropic trubulence. *Annu. Res. Briefs*, pp. 461–473, Stanford University/NASA Ames.

Peters, N. 2000 *Turbulent Combustion.* Cambridge University Press.

Poinsot, T. J. & Lele, S. K. 1992 Boundary conditions for direct numerical simulations of compressible viscous flows. *J. Comput. Phys.* **101**, 104–129.

Pope, S. B. 1988 The evolution of surfaces in turbulence. *Intl J. Engng Sci.* **28**, 445–469.

Pope, S. B. 1990 Computation of turbulent combustion: progress and challenges. *Proc. Combust. Inst.* **23**, 591–612.

Pope, S. B. 2000 *Turbulent Flows*. Cambridge University Press.

Pope, S. B. & Ching, E. S. C. 1993 Stationary probability density functions: an exact result. *Phys. Fluids* A **5**, 1529–1531.

Rosales, C. & Meneveau, C. 2005 Linear forcing in numerical simulations of isotropic turbulence: physical space implementations and convergence properties. *Phys. Fluids* **17**, 095106.

Shepherd, I. G. & Kostiuk, L. W. 1994 The burning rate of premixed turbulent flames in divergent flows. *Combust. Flame* **96**, 371–380.

Swaminathan, N., Bilger, R. W. & Ruetsch, G. R. 1997 Interdependence of the instantaneous flame front structure and the overall scalar flux in turbulent premixed flames. *Combust. Sci. Tech.* **128**, 73–97.

Swaminathan, N., Bilger, R. W. & Cuenot, B. 2001 Relationship between turbulent scalar flux and conditional dilatation in premixed flames with complex chemistry. *Combust. Flame* **126**, 1764–1779.

Thévenin, A. 2005 Three-dimensional direct simulations and structure of expanding turbulent methane flames. *Proc. Combust. Inst.* **30**, 629–637.

Trouve, A. & Poinsot, T. J. 1994 The evolution for the flame surface density. *J. Fluid Mech.* **278**, 1–26.

Vervisch, L., Bidaux, E., Bray, K. N. C. & Kollmann, W. 1995 Surface density function in premixed turbulent combustion modeling, similarities between probability density function and flame surface approaches. *Phys. Fluids* **7**, 2496–2503.

Veynante, D. & Poinsot, T. J. 1997 Effects of pressure gradients on turbulent premixed flames. *J. Fluid Mech.* **353**, 83–114.

Zimont, V. L. 1979 Theory of turbulent combustion of a homogeneous fuel mixture at high Reynolds numbers. *Combust. Explos. Shock Waves* **15**, 305–311.